Localized standing waves in inhomogeneous Schrödinger equations

2010 Nonlinearity 23 2059

(http://iopscience.iop.org/0951-7715/23/9/002)

IOP PUBLISHING NONLINEARITY

Nonlinearity **23** (2010) 2059–2080 doi:10.1088/0951-7715/23/9/002

Localized standing waves in inhomogeneous Schrödinger equations

R Marangell[1,2], C K R T Jones[1,2] and H Susanto[3]

[1] Department of Mathematics, University of North Carolina at Chapel Hill, Chapel Hill, NC 27599, USA
[2] Mathematics Institute, Zeeman Building, University of Warwick, Coventry, CV4 7AL, UK
[3] School of Mathematical Sciences, University of Nottingham, University Park, Nottingham, NG7 2RD, UK

E-mail: hadi.susanto@nottingham.ac.uk

Received 18 February 2010, in final form 28 June 2010
Published 29 July 2010
Online at stacks.iop.org/Non/23/2059

Recommended by M J Peyrard

Abstract

A nonlinear Schrödinger equation arising from light propagation down an inhomogeneous medium is considered. The inhomogeneity is reflected through a non-uniform coefficient of the nonlinear term in the equation. In particular, a combination of self-focusing and self-defocusing nonlinearity, with the self-defocusing region localized in a finite interval, is investigated. Using numerical computations, the extension of linear eigenmodes of the corresponding linearized system into nonlinear states is established, particularly nonlinear continuations of the fundamental state and the first excited state. The (in)stability of the states is also numerically calculated, from which it is obtained that symmetric nonlinear solutions become unstable beyond a critical threshold norm. Instability of the symmetric states is then investigated analytically through the application of a topological argument. Determination of instability of positive symmetric states is reduced to simple geometric properties of the composite phase plane orbit of the standing wave. Further the topological argument is applied to higher excited states and instability is again reduced to straightforward geometric calculations. For a relatively high norm, it is observed that asymmetric states bifurcate from the symmetric ones. The stability and instability of asymmetric states is also considered.

Mathematics Subject Classification: 37K40, 37K45, 37K50

(Some figures in this article are in colour only in the electronic version)

1. Introduction

Inhomogeneities can act as an effective trapping to collective excitations in nonlinear media. In the field of nonlinear integrated optics, the first theoretical works on guided waves by an interface between a linear and nonlinear medium appeared in [1, 23, 24, 39]. Various stationary wave profiles propagating along nonlinear planar optical guides in a layered structure are then extensively considered (see, e.g., [2, 4, 14, 31, 34] and references therein). When the inhomogeneities are periodic, one will obtain discrete waveguide arrays, which have become an independent topic of interest [21]. A next fundamental question is whether or not the standing waves are stable to propagation along the nonlinear waveguide.

The stability of stationary nonlinear Schrödinger waves in homogeneous media was first considered by Vakhitov and Kolokolov [17, 44]. Using variational arguments, a criterion was derived relating the soliton linear stability and the slope of the corresponding power-dispersion curve, i.e. the known Vakhitov–Kolokolov condition. The method was later rigorously justified in [10, 45]. Subsequent studies extend the condition for various situations, including inhomogeneous problems [15, 25, 40–43] (see also a recent brief review [33] and references therein).

An interesting waveguide system was proposed in [41], consisting of a self-focusing Schrödinger equation and a self-defocusing type inhomogeneity with finite length. It is experimentally feasible to fabricate such a waveguide using the current technology as self-focusing and self-defocusing can be achieved in the same medium, structure and wavelength [26]. In the context of a Bose–Einstein condensation [3, 5, 6, 8, 9], which is also modelled by a nonlinear Schrödinger equation [11, 28], such a sign-changing nonlinearity coefficient can be created by spatially varying the condensate's atomic scattering length making the so-called collisionally inhomogeneous nonlinearity [30, 37, 38]. By engineering the scattering length, one can make a controllable emission of matter-wave bursts from a Bose–Einstein condensate [29]. Combining a spatially varying nonlinearity coefficient with a harmonic trap can also create nontrivial properties, such as multistable configurations of the condensate density as well as a pair of stable ground states corresponding to the same parameter values [46].

Tran [41] extended the work of, e.g., [2, 15], in which the inhomogeneity is linear. In [41] the self-defocusing inhomogeneity has a small nonlinearity coefficient, such that the characteristics of the stationary solutions are closely related to the corresponding linear problem. The system was later studied by Leon [22], where the nonlinearity coefficient of the inhomogeneity was of the same order as the self-focusing regions. Analytical solutions of stable symmetric solutions below a threshold amplitude were derived in terms of Jacobian elliptic functions [22].

We study the existence and stability of symmetric and asymmetric solutions, particularly the fundamental and the first excited mode, when the nonlinearity coefficient of the defocusing inhomogeneity is of the same order as the focusing bounding regions. We show that continuing from the linear limit solutions, there is a saddle-node bifurcation at which the symmetric mode becomes unstable and asymmetric modes emerge. Even though it is similar to the results reported in [41], there is a significant difference where the asymmetric positive solutions are all stable in their existence region. Moreover, [41] only considers positive solutions. Besides determining the instability of symmetric solutions numerically, we also show it analytically using topological argument techniques as developed in [15, 16]. We also comment on the inapplicability of the analytical techniques to asymmetric solutions.

In section 2, the governing equations are discussed and the corresponding linear eigenvalue problem is derived. In section 3, we consider the linear limit of the equations, where a transcendental equation determining the bifurcation points of non-uniform solutions from the

uniform solution $u = 0$ is derived. In the same section, numerical continuations of the fundamental and the first excited state from the linear limit to nonlinear states are presented. The linear (in)stability of the numerically obtained (symmetric and asymmetric) solutions is then determined numerically by solving the corresponding linear eigenvalue problem. The instability of the symmetric solutions are analysed analytically in section 4 using a topological argument. In section 5 we consider some asymmetric solutions.

2. Mathematical model

We consider the following governing system of differential equations

$$\begin{aligned} &\mathrm{i}\Psi_t + \Psi_{xx} + |\Psi|^2\Psi = V\Psi \qquad |x| > L, \\ &\mathrm{i}\Psi_t + \Psi_{xx} - \eta|\Psi|^2\Psi = 0 \qquad |x| < L, \end{aligned} \tag{1}$$

where the 'outer' and the 'inner' equation has focusing and defocusing ($\eta > 0$) type nonlinearity, respectively, and L is a positive real parameter representing half the length of the waveguide. The particular case of a point defect $L \to 0$ has been considered in [35]. The norm

$$N = \int_{-\infty}^{\infty} |\Psi(x,t)|^2 \,\mathrm{d}x,$$

which is physically related to the intensity power of the electromagnetic field in the context of nonlinear optics or the number of atoms in Bose–Einstein condensates is conserved.

To study standing waves of (1), we pass to a rotating frame and consider solutions of the form $\Psi(x,t) = \mathrm{e}^{-\mathrm{i}\omega t}\psi(x,t)$. We then have

$$\begin{aligned} &\mathrm{i}\psi_t + \psi_{xx} + |\psi|^2\psi = (V-\omega)\psi \qquad |x| > L, \\ &\mathrm{i}\psi_t + \psi_{xx} - \eta|\psi|^2\psi = -\omega\psi \qquad |x| < L. \end{aligned} \tag{2}$$

Standing wave solutions of (1) will be steady-state solutions to (2). For rigorous results concerning the existence of such solutions see, for example, [7, 13, 36]. In the following, the parameter η is taken to be $\eta = 1$. We consider real, t independent solutions $u(x)$ to the ODE:

$$\begin{aligned} &u_{xx} = (V-\omega)u - u^3 \qquad |x| > L, \\ &u_{xx} = -\omega u + u^3 \qquad |x| < L. \end{aligned} \tag{3}$$

To obtain solutions that decay to 0 as $x \to \pm\infty$, the condition that $V - \omega > 0$ is required, with $\omega \in \mathbb{R}$. We will also require that $u_x \to 0$ as $x \to \pm\infty$. To establish the instability of a standing wave solution we linearize (2) about a solution to (3). Writing $\psi = u(x) + \epsilon\left((r(x) + \mathrm{i}s(x))\mathrm{e}^{\lambda t} + (r(x)^\star + \mathrm{i}s(x)^\star)\mathrm{e}^{\lambda^\star t}\right)$ and retaining terms linear in ϵ leads to the eigenvalue problem

$$\lambda\begin{pmatrix} r \\ s \end{pmatrix} = \begin{pmatrix} 0 & D_- \\ -D_+ & 0 \end{pmatrix}\begin{pmatrix} r \\ s \end{pmatrix} = M\begin{pmatrix} r \\ s \end{pmatrix}, \tag{4}$$

where the linear operators D_+ and D_- are defined as

$$D_+ = \begin{cases} \dfrac{\partial^2}{\partial x^2} - (V-\omega) + 3u^2, & |x| > L, \\ \dfrac{\partial^2}{\partial x^2} + \omega - 3u^2, & |x| < L, \end{cases} \tag{5}$$

$$D_- = \begin{cases} \dfrac{\partial^2}{\partial x^2} - (V-\omega) + u^2, & |x| > L, \\ \dfrac{\partial^2}{\partial x^2} + \omega - u^2, & |x| < L. \end{cases} \tag{6}$$

It is then clear that the presence of an eigenvalue of M with positive real part implies instability.

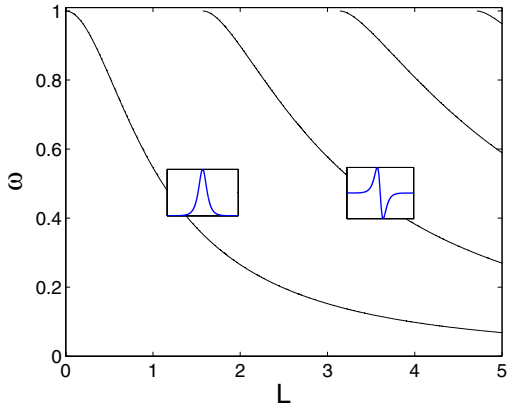

Figure 1. Bifurcation points of non-uniform solutions from the zero solution $u \equiv 0$ in the (L, ω)-plane for $V = 1$. The insets present a sketch of the corresponding solution $u(x)$ along the first two branches.

3. Linear states and their continuation: numerical results

In the small limit of $u(x)$, the governing equation (3) is reduced to the linearized system

$$\begin{aligned} u_{xx} &= (V-\omega)u \qquad |x| > L, \\ u_{xx} &= -\omega u \qquad\quad |x| < L, \end{aligned} \tag{7}$$

which can be simply solved analytically to yield

$$u(x) = \begin{cases} \mathrm{e}^{-\sqrt{V-\omega}|x|}, & x < -L, \\ c_e \cos(\sqrt{\omega}x) + c_o \sin(\sqrt{\omega}x), & |x| < L, \\ c_r e^{-\sqrt{V-\omega}|x|}, & x > L. \end{cases} \tag{8}$$

From the natural continuity conditions at the points of discontinuity

$$u(\pm L^+) = u(\pm L^-),\ u_x(\pm L^+) = u_x(\pm L^-),$$

one will obtain that the parameters of the linear states above will have to satisfy the transcendental equation

$$\sqrt{V-\omega}\left(1 - 2\cos^2(\sqrt{\omega}L)\right) = \frac{1}{2}\left(\frac{V}{\sqrt{\omega}} - 2\sqrt{\omega}\right)\sin(2\sqrt{\omega}L). \tag{9}$$

This equation determines bifurcation points of non-uniform states from the zero solution. A plot of (9) for $V = 1$ is given in figure 1.

Starting from a bifurcation point, as the parameter ω varies, the corresponding linear limit solution will deform and nonlinear terms will play a role. Even though one can still represent the continued solutions in terms of the Jacobian elliptic functions [22], here we solely use numerical computations. A pseudo-arclength method is used to follow the existence curve of a solution as a parameter is varied. We have solved equations (3) and (4) numerically to study the existence and the stability of localized standing waves, where a central finite difference is used to approximate the Laplacian with a relatively fine discretization. In particular, we consider the first two branches of linear limits shown in figure 1.

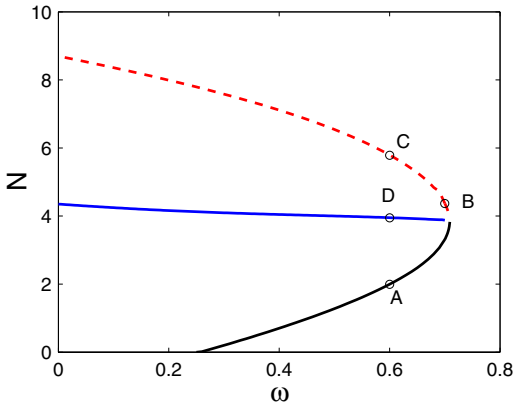

Figure 2. The norm N as a function of ω for the first (positive) state corresponding to the first branch in figure 1. As ω increases from the bifurcation point $\omega \approx 0.265$, there is a bifurcation at which the state becomes unstable. In addition to the symmetric positive states, there is also a stable asymmetric state along the middle (solid blue) branch. Solid and dashed curve represents stable and unstable solutions, respectively.

3.1. Positive solutions

First, we consider the continuation of the linear state corresponding to the first branch. For illustrative purposes, we take $V = 1$ and $L = 2$, i.e. the fundamental state mode originates from $\omega \approx 0.265$. In figure 2, we present the numerically obtained continuation of the linear positive solution as ω varies.

At the bifurcation point, the linear state is expected to be stable, similar to the zero uniform state $u(x) \equiv 0$. As ω increases, the norm N of the solution increases as well. By appealing to the work of [10, 32, 45], we obtain that the solution along this branch is stable. In figure 3(a), we depict a solution corresponding to point A in figure 2 and its eigenvalue structure in the complex plane, where one can see that all the eigenvalues are on the imaginary line.

As the parameter ω is increased further, there is a bifurcation at which the existence curve reverses direction. Symmetric solutions are unstable along this branch. Two solutions and their eigenvalues in the complex plane corresponding to point B and C are shown in figures 3(b) and (c), respectively. One can note that the instability of the solutions are due to the presence of a pair of eigenvalues with nonzero real part.

Interestingly, in addition to the symmetric states, at the bifurcation point where symmetric states become unstable, there is an existence curve emerging, corresponding to some numerically stable asymmetric states. A solution indicated as point D in figure 2 is presented in figure 3(d).

Figure 2 is similar to figure 1 in [41], which is for the case of relatively small $\eta > 0$. Writing $(V - \omega) \to W^2$ and $-\omega \to (W^2 - V^2)$ and $L = 1$, the time independent system of (2) becomes the same as equation (1) in [41]. One important difference is that in our case, asymmetric solutions are all (at least numerically) stable in their existence domain.

When a solution is unstable, it is certainly of interest to see the dynamics near it. Here, we have solved the time-dependent governing equation (1) using a Runge–Kutta method. Depicted in figures 4(a) and (b) are the dynamics of solution (b) and (c) in figure 3, respectively, perturbed initially by small random disturbances. Shown is the modulus $|\psi(x, t)|^2$. One can clearly see that the instability of solution in figure 3(b) manifests in the form of spontaneous symmetry breaking, while the instability of the solution in figure 3(c) is in the form of a soliton generation, similar to that reported before in [22].

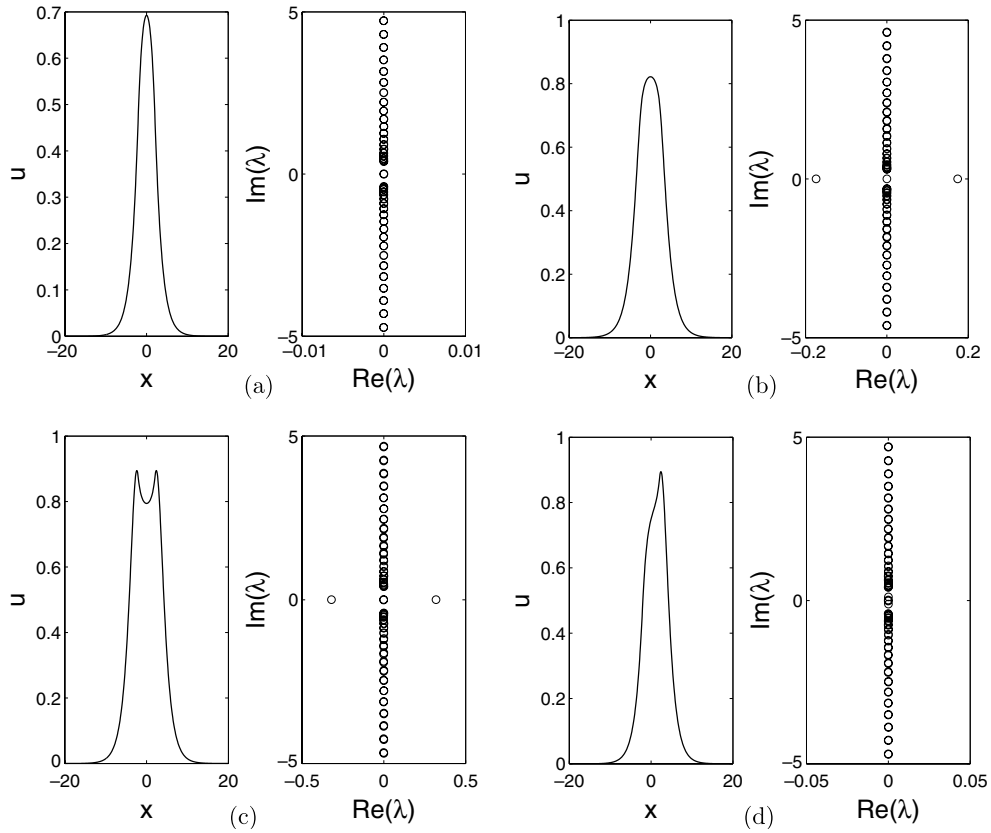

Figure 3. Profile of solutions at points indicated as A–D in figure 2 and their eigenvalue structures in the complex plane. The phase portraits of the solutions in each panel are presented in figure A1.

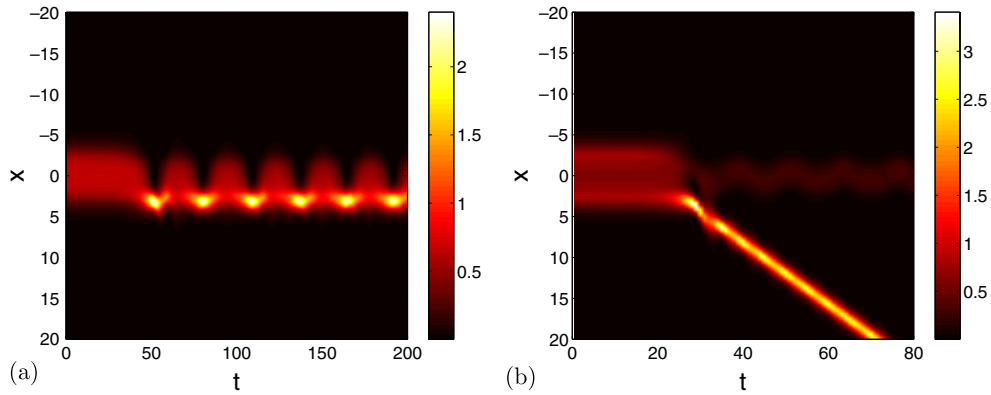

Figure 4. Time dynamics of solutions at points indicated as B and C in figure 2. Shown is the top view of $|\Psi(x,t)|^2$.

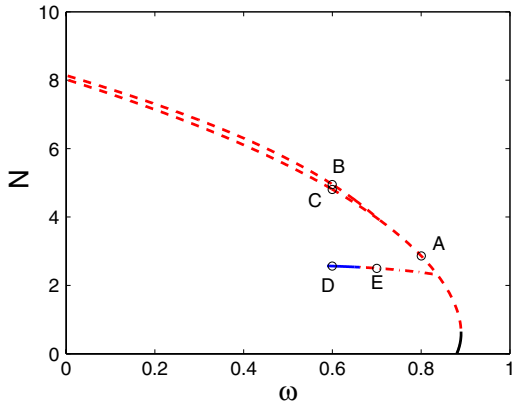

Figure 5. The same as figure 2, but for the first excited state, corresponding to the second branch in figure 1. The bifurcation point of the linear state is $\omega \approx 0.898$.

3.2. First excited state

We have considered as well solutions bifurcating from the first excited state corresponding to the second branch in figure 1. For the same V and L as above, this state bifurcates from the point $\omega \approx 0.898$. We depict in figure 5 the continuation of this state as ω varies.

As the parameter ω increases from the bifurcation point, one will obtain a numerically stable symmetric state. When the parameter is increased further, there will also be a 'direction reversal' point, where the symmetric state becomes unstable, similar to the case of fundamental state solutions above. Shown in figure 6(*a*) is an example of this state and its spectrum in the complex plane.

Besides similarities with the previous case, we also observed several differences here. These include the fact that there are now more than one existence branches corresponding to asymmetric solutions. Presented in figure 6(*b*) is a solution along the first asymmetric branch, indicated as point B in figure 5, and its eigenvalue structure. As a comparison, we also plot in figures 6(*c*) and (*d*) the symmetric and asymmetric solution from point C and D in figure 5, respectively, and their eigenvalues in the complex plane.

The two asymmetric solutions from point B and D above are clearly different. By viewing this first excited state as composed of two static out-of-phase solitons, the asymmetric solution B can be seen as composed of two solitons with one of them spatially displaced, while the solution D can be viewed as composed of two solitons with different amplitudes.

It is also interesting to note that the asymmetric solution D is not always numerically unstable in its existence region. Numerically, we observed a region of stability and of instability for this asymmetric state, depicted as a solid and dashed line, respectively, in figure 5. In figure 6(*e*), we present an unstable asymmetric state and its spectra, where one can see the presence of two pairs of eigenvalues with nonzero real part.

Typical time dynamics of unstable solutions for this case is presented in figure 7. In particular, we plot the dynamics of asymmetric solutions B and E under random perturbations. The dynamics in time of solution C is similar to that of solution B.

4. Unstable symmetric solutions past the bifurcation point

In the following, we will analytically prove the instability of symmetric solutions past the 'direction reversal' point above. To show instability of the standing waves, we will show that

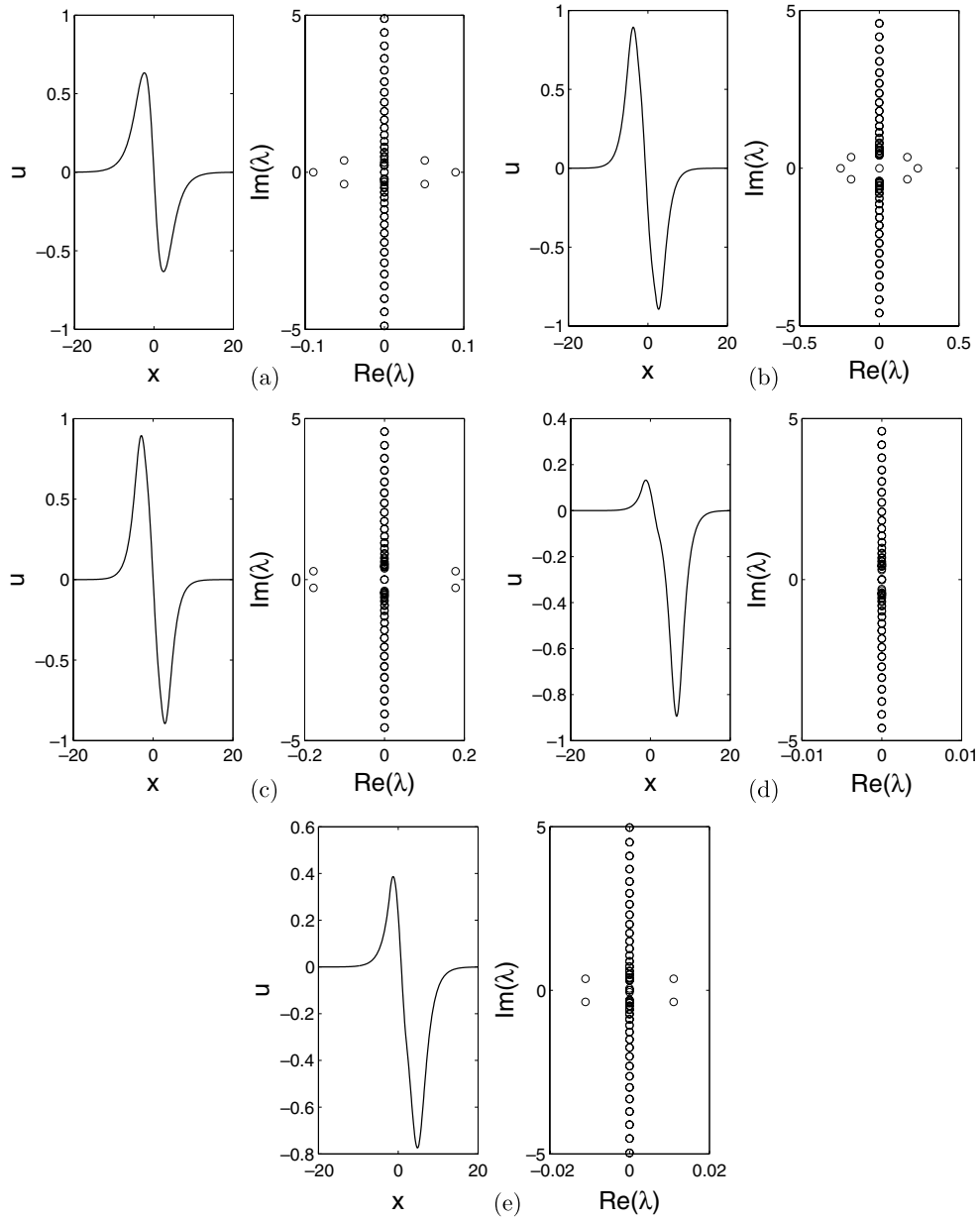

Figure 6. Profile of solutions and their corresponding eigenvalue structure in the complex plane at points indicated as A–D in figure 5. The solution phase portraits are shown in figure A2.

M has a real positive eigenvalue. This is done by applying the main theorem of [16]. As in [16], the domains of the operators D_- and D_+ will be $H^1(\mathbb{R})$. We directly compare the analytical results with numerical evidence in the remarks.

It can be shown that the following quantities are well defined (see [16]):

$$P = \text{ the number of positive eigenvalues of } D_+,$$
$$Q = \text{ the number of positive eigenvalues of } D_-.$$

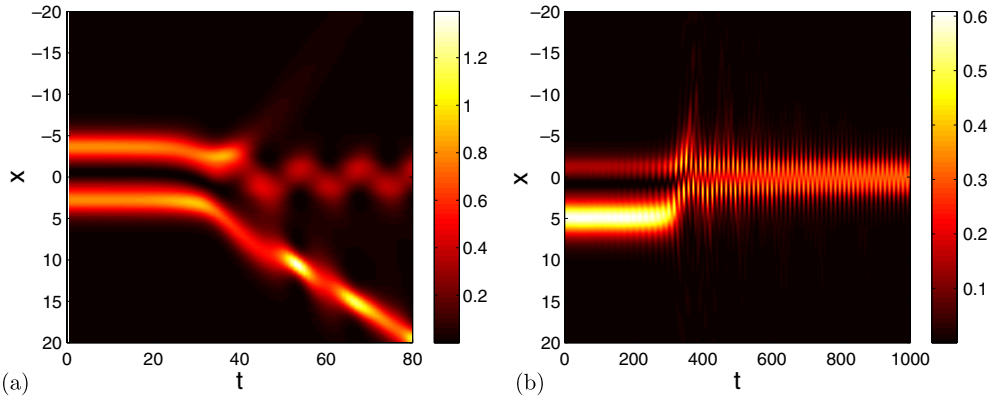

Figure 7. The dynamics in time of solutions at points indicated as B and E in figure 5, respectively. Shown is the top view of $|\Psi(x,t)|^2$.

We then have the following:

Theorem 1 ([16]). *If $P - Q \neq 0, 1$, there is a real positive eigenvalue of the operator M.*

From Sturm–Liouville theory, P and Q can be determined by considering solutions of $D_+v = 0$ and $D_-v = 0$, respectively. In fact, they are the number of zeros of the associated solution v. Note that $D_-v = 0$ is actually satisfied by the standing wave itself, and that $D_+v = 0$ is the equation of variations of the standing wave equation. It follows that

$$Q = \text{ the number of zeros of the standing wave } u(x).$$
$$P = \text{ the number of zeros of a solution to the variational equation along } u(x).$$

We will focus first on the case when we have a positive localized steady-state solution, i.e. $Q = 0$.

4.1. Positive solutions

The idea is to use a dynamical systems point of view and geometric properties of the solution curves in the phase portrait to establish when $P \geqslant 2$. The t independent solutions to equation (2) can be represented by composite phase portraits constructed by a superpositioning of the phase portraits of the 'outer' system:

$$u_x = y, \qquad y_x = (V - \omega)u - u^3, \tag{10}$$

and the 'inner' one:

$$u_x = y, \qquad y_x = -\omega u + u^3. \tag{11}$$

We can view the composite picture as a single, non-autonomous system with phase plane given by

$$u_x = y,$$
$$y_x = \begin{cases} (V - \omega)u - u^3, & |x| > L, \\ -\omega u + u^3, & |x| < L. \end{cases} \tag{12}$$

In the phase plane of (10), the outer system admits a soliton solution, given by the equation

$$y^2 = (V - \omega)u^2 - \frac{u^4}{2}, \tag{13}$$

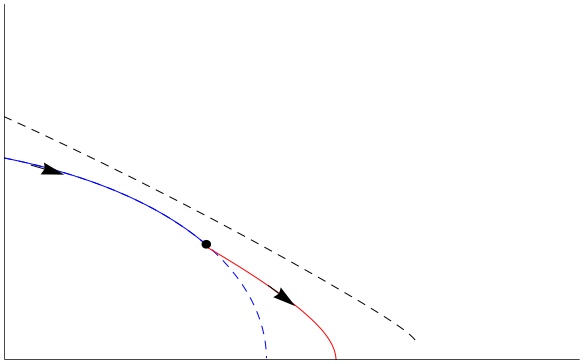

Figure 8. Part of an unstable orbit that appears when the heteroclinic orbit of the inner system (the black dashed line given by equation (14)) is 'close' relative to the homoclinic orbit of the inner system (the blue/lower dashed line given by equation (13)). The dot represents the jumping off point. The black arrows represent the direction of travel in the phase plane. The orbit follows first the blue curve and then jumps to the red/lower curve. As ω/V decreases the blue dashed line will cross the black dashed line and unstable orbits of the second type will appear (see figure 9(*b*) for an example of such an orbit).

while the inner system (11) admits a heteroclinic orbit in the phase plane given by

$$y^2 = -\omega u^2 + \frac{u^4}{2} + \frac{\omega^2}{2}. \tag{14}$$

The conditions that u and u_x decay to zero as x goes to $\pm\infty$ mean that in the superposed phase portraits all steady-state solutions that we are interested in will lie on the soliton curve as $x \to \pm\infty$.

Solution curves of the inner system are given by

$$y^2 = -\omega u^2 + \frac{u^4}{2} + C. \tag{15}$$

The solutions we are interested in will travel in the phase plane out from the origin along the homoclinic orbit of the outer system described by (13) and then 'flip' to the inner system for $2L$ units of x and then 'flip' back to the outer system along the homoclinic orbit. Define (u_0, y_0) as the point in the phase plane of (12) where the solution initially flips from the outer to the inner system, and define (u_1, y_1) as the point in the phase plane where the solution returns to the outer system. Using this notation we can write the equation of the part of the solution curve in the inner system in the (composite) phase plane as

$$y^2 = -\omega u^2 + \frac{u^4}{2} + V u_0^2 - u_0^4. \tag{16}$$

As the parameters V and ω vary, the relative position of the homoclinic orbit described by (13) and the heteroclinic orbit described in (14) will change. We consider the qualitative and numerical differences that occur for various values of L corresponding to different configurations of the potential V and the frequency ω. Namely when the curves described by (14) and (13) are 'close' together (cf figure 8), linearly unstable standing wave solutions to (1) appear.

Theorem 2. *Unstable positive localized solutions to (1) occur whenever* $\omega/V < 3/4$. *The unstable positive symmetric solutions are the ones which are symmetric in the phase plane with respect to the u-axis and leave the homoclinic orbit at a point* (u_0, y_0) *satisfying* $\sqrt{V/2} < u_0$.

The theorem will be proved by showing that $P \geqslant 2$ for such a solution. From Sturm–Liouville theory we have that P will be the number of zeros of a solution to the variational equation $D_+v = 0$ satisfying the boundary conditions $v \to 0$ as $x \to -\infty$. A solution to the variational equation associated with a solution of (3) can be found by following a tangent vector around the orbit under the flow of the linear equations (19). Satisfying the initial conditions means the solution will be a tangent vector to the orbit of the solution of (3) in the phase plane until the discontinuity of (3). The number of zeros of such a solution can be found by determining the number of times that such a vector must pass through the vertical as the base point ranges over the entire orbit.

Denote by $b^O(u, y) = (b_1^O(u, y), b_2^O(u, y))$ a tangent vector to the homoclinic orbit of the outer system at the point (u, y), and let $b^I(u, y) = (b_1^I(u, y), b_2^I(u, y))$, be a tangent vector to an orbit of the inner system at the point (u, y). As (u, y) varies along the homoclinic orbit, $b^O(u, y) = (p, q)$ solves the linear system:

$$\begin{aligned} p_x &= q, \\ q_x &= (V - \omega)p - 3u^2 p, \end{aligned} \tag{17}$$

while $b^I(u, y)$ solves the linear system:

$$\begin{aligned} p_x &= q, \\ q_x &= -\omega p + 3u^2 p, \end{aligned} \tag{18}$$

as (u, y) travels along a curve given by (15) the composite linear variational equation is then given by

$$\begin{aligned} p_x &= q, \\ q_x &= \begin{cases} (V - \omega)p - 3u^2 p, & |x| > L, \\ -\omega p + 3u^2 p, & |x| < L. \end{cases} \end{aligned} \tag{19}$$

We denote the explicit vectors, $b^O(u_0, y_0)$ and $b^I(u_1, y_1)$, by β^O and β^I, respectively. Let F^O and F^I denote the flow of the outer (10) and inner (11) systems, respectively, and Φ^O and Φ^I denote the variational flow of the outer and inner systems along solutions. If $d(u, y) = (d_1(u, y), d_2(u, y))$ is a vector in the tangent space of the phase plane at the point (u, y), and if (u, y) is flowed under F^O and F^I to $F^O(u, y)$ and $F^I(u, y)$, respectively, let $\Phi^O(d)(F^O(u, y))$, $\Phi^I(d)(F^I(u, y))$ denote the image of the vector d under the flow of the outer and inner variational systems, respectively.

Before moving to the proof of the theorem we need two geometric facts about the flows Φ^O and Φ^I. For further reference and proofs of the following see, for example, [12] or [27].

Fact 1. *The variational flows Φ^O and Φ^I map the tangent line to a solution to (10) and (11) at a point (u, y), to the tangent space of the solution at the point $F^O(u, y)$ and $F^I(u, y)$, respectively.*

Fact 2. *The flows Φ^O and Φ^I are orientation preserving.*

This second fact is reflected in the following way; if $b(u, y) = (b_1(u, y), b_2(u, y))$ and $d(u, y) = (d_1(u, y), d_2(u, y))$ are two vectors tangent to the phase space at (u, y), then the sign of the cross product of the two vectors is unchanged under the flows. That is

$$\operatorname{sgn}(b(u, y) \times d(u, y)) = \operatorname{sgn}(\Phi^O(b)(F^O(u, y)) \times \Phi^O(d)(F^O(u, y))) \tag{20}$$

for every point in the orbit of the flow F^O. The above also holds with the outer flow replaced by the inner flow.

A consequence of these two facts for the system of interest is the following lemma:

Lemma 3. *If $d(u, y)$ is a vector in the tangent space to the phase plane of the homoclinic orbit at the point (u, y), with $u > 0$ such that $d(u, y) \times b^O(u, y) > 0$, then*

$$\lim_{x\to\infty} \Phi^O\left(\frac{d}{|d|}\right)(F^O(u, y)) = k\begin{pmatrix} 1 \\ \sqrt{V-\omega} \end{pmatrix} \tag{21}$$

where k is a positive real number.

Proof. Because $b^O(u, y)$ is a tangent vector to the homoclinic orbit, and $u > 0$,

$$\lim_{x\to\infty} \Phi^O\left(\frac{b^O}{|b^O|}\right)(F^O(u, y)) = \lim_{x\to\infty} \frac{b^O}{|b^O|}(F^O(u, y)) = \frac{1}{\sqrt{1+V-\omega}}\begin{pmatrix} -1 \\ \sqrt{V-\omega} \end{pmatrix} \tag{22}$$

and since d is not tangent to the homoclinic orbit,

$$\lim_{x\to\infty} \Phi^O\left(\frac{d}{|d|}\right)(F^O(u, y)) = k\begin{pmatrix} 1 \\ \sqrt{V-\omega} \end{pmatrix}, \tag{23}$$

where k is some real number. This is because $\begin{pmatrix} 1 \\ \sqrt{V-\omega} \end{pmatrix}$ is the unstable asymptotic eigenvector of (17). But from the first and second fact we have that

$$0 < \lim_{x\to\infty} \Phi^O\left(\frac{d}{|d|}\right)(F^O(u, y)) \times \frac{b^O}{|b^O|}(F^O(u, y)) = \frac{2k\sqrt{V-\omega}}{\sqrt{1+V-\omega}}, \tag{24}$$

which means that k must be positive. □

In order to determine the number of zeroes of a solution to $D_+v = 0$ and $v \to 0$ as $x \to -\infty$, we need to determine the number of times a vector gets pushed through the vertical by the flow as its base point moves along the orbit. In order to count this, we break the orbit up into three parts. These are when $x < -L$, $|x| < L$ and $x > L$. Let A_1 denote the number of zeros of the solution to the variational equation as the basepoint corresponds to the range $x < -L$, A_2 the number for $|x| < L$ and A_3 for $x > L$. We have the following:

- The number A_1 is the number of times $b^O(u, y)$, a vector tangent to the homoclinic orbit passes through the vertical as (u, y) travels from $(0, 0)$ along the homoclinic orbit of the outer system to the point (u_0, y_0).
- The number A_2 is the number of times $\Phi^I(\beta^O)(u, y)$ passes through the vertical as (u, y) travels from (u_0, y_0) along the path $y^2 = u^4/2 - \omega u^2 + Vu_0^2 - u_0^4$ to the point (u_1, y_1).
- The number A_3 is the number of times $\Phi^O(\Phi^I(\beta^O)(u_1, y_1))(u, y)$ passes through the vertical as (u, y) travels along the homoclinic orbit of the outer system from (u_1, y_1) to $(0, 0)$.

The number of zeros of a solution of (19) will then be $P = A_1 + A_2 + A_3$. Theorem 1 then says that if $u(x) > 0$ and if $A_1 + A_2 + A_3 \geqslant 2$, then the underlying orbit in the phase plane represents an unstable standing wave solution of (1). We are now ready to prove theorem 2.

Proof of theorem 2. We have two cases to consider, the first is when $\sqrt{V/2} < u_0 < \sqrt{\omega}$ and the second is when $u_0 > \sqrt{\omega}$. In both cases, however, $u_0 > \sqrt{V-\omega}$.

Case 1. Here $\sqrt{V/2} < u_0 < \sqrt{\omega}$. An example is as in figure 9(*a*). Note that in this case $y_0 > 0$. We show that $A_2 \geqslant 1$ and $A_2 + A_3 \geqslant 2$, so the solution represents an unstable standing wave. First we show that $A_2 \geqslant 1$. Note that $\beta^O = (y_0, (V-\omega)u_0 - u_0^3)$, and that the first coordinate is positive while the second coordinate of β^O is negative since $V/2 < u_0 < \sqrt{\omega}$. Now note that $b^I(u_0, y_0) = (y_0, u_0^3 - \omega u_0)$, and again in the second coordinate we have that

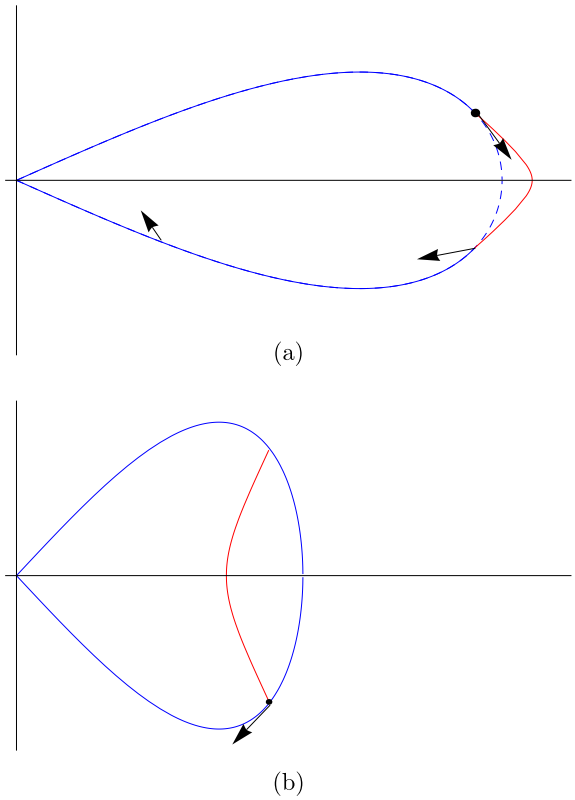

Figure 9. (*a*) An unstable orbit of the first type. The dashed line is the homoclinic orbit of the outer system. The dot represents the jumping off point. The black arrows represent the image of a tangent vector to a solution under the variational flows $\Phi^{O,I}$ at various values. (*b*) An unstable orbit of the second type. The dot represents the jumping off point. The black arrow represents where $\Phi(b^O)$ stops being tangent to the orbit of the solution.

$u_0 > \sqrt{V-\omega}$. This means that $\beta^O \times b^I(u_0, y_0) = y_0 u_0(2u_0^2 - V) > 0$, because $u_0 > \sqrt{V/2}$ and y_0 is positive. Now we flow both vectors along the inner system until we get to the point where the solution to the original equation crosses the u-axis in the phase plane of the system described by (12). Denote this point by $(u_{\max}, 0)$. We then have the following:

$$0 < \Phi^I(\beta^O)(u_{\max}, 0) \times b^I(u_{\max}, 0) = (u_{\max}^3 - \omega u_{\max})\Phi_1^I(\beta^O)(u_{\max}, 0).$$

Since $u_0 < \sqrt{w}$ this means that $u_{\max} = \sqrt{\omega - \sqrt{\omega^2 + 2(Vu_0^2 + u_0^4)}} < \sqrt{\omega}$ and so the first coordinate of $\Phi^I(\beta^O)(u_{\max}, 0)$, $\Phi_1^I(\beta^O)(u_{\max}, 0) < 0$. But this means that the flow has pushed the original tangent vector to the homoclinic orbit through the vertical at least once by this point, since the sign of the first coordinate has changed, so $A_2 \geqslant 1$.

To study A_3, we must determine the number of times that $\Phi^O(\Phi^I(\beta^O)(u_1, y_1))(u, y)$ passes through the vertical as the base point travels along the homoclinic orbit from (u_1, y_1) to $(0, 0)$. We first apply the result of the lemma to the vector β^I. Observe that $\beta^I = (-y_0, u_0^3 - \omega u_0)$, (since in this case $(u_1, y_1) = (u_0, -y_0)$) and that the first and second coordinates of β^I are negative. Now $\beta^I \times b^O(u_1, y_1) = y_1(Vu_1 - 2u_1^3) > 0$, since $u_1 = u_0 > \sqrt{V/2}$. So applying the result of lemma 3 means that there is a point on the homoclinic orbit (u', y') say, where $\Phi^O(\beta^I)(u', y')$ is pointing vertically upwards. Write

$\Phi^O(\beta^I)(u', y') := (0, a)$, with a positive. Now we apply the fact that the variational flows are orientation preserving. We have

$$0 < \Phi^O(\Phi^I(\beta^O)(u_1, y_1))(u', y') \times (0, a) = a(\Phi_1^O(\Phi^I(\beta^O)(u_1, y_1))(u', y'))$$

which means that the first coordinate of $\Phi^O(\Phi^I(\beta^O)(u_1, y_1))(u', y')$ must be positive at this point. The first coordinate under the variational flow $\Phi_1^I(\beta^O)$ was shown to be negative above, so this means that the vector $\Phi^I(\beta^O)$ must have either passed through the vertical once more, or been pushed through the vertical by Φ^O, by this point, so $A_2 + A_3 \geqslant 2$.

Thus we have that the number of zeros to the variational equation must be greater than or equal to two, so the corresponding orbit must represent an unstable standing wave.

Case 2. In this instance $u_0 > \sqrt{\omega}$. An example of the phase portrait of an orbit of this type is in figure 9(*b*). Here we remark that since $u_0 > \sqrt{\omega}$ this means that y_0 must be negative. In this case we show that $A_1 \geqslant 1$ and that $A_1 + A_2 + A_3 \geqslant 2$.

To see that $A_1 \geqslant 1$, we note that the tangent line to the homoclinic orbit is vertical when the homoclinic orbit crosses the u-axis. As the base point moves along the homoclinic orbit from $(0, 0)$ to (u_0, y_0), it must cross the u-axis, so $A_1 \geqslant 1$.

Now we study A_3. Call the point where the homoclinic orbit crosses the u-axis $(u_{\max}, 0)$. Note that $\beta^O = (y_0, (V - w)u_0 - u_0^3)$ and that the sign of the first coordinate is negative. The sign of $\Phi^I(\beta^O)(u_1, y_1) \times b^O(u_1, y_1)$ can be either positive, negative or zero. If it is positive apply lemma 3 to see that

$$\lim_{x\to\infty} \frac{\Phi^O(\Phi^I(\beta^O)(u_1, y_1))(u, y)}{|\Phi^O(\Phi^I(\beta^O)(u_1, y_1))(u, y)|} = \begin{pmatrix} k \\ k\sqrt{V - \omega} \end{pmatrix},$$

where k is positive, so the flow must have pushed the vector through the vertical once more, since the first coordinate in the limiting vector is positive. Thus $A_1 + A_2 + A_3 \geqslant 2$.

If $\Phi^I(\beta^O)(u_1, y_1) \times b^O(u_1, y_1) = 0$, then $\Phi^I(\beta^O)(u_1, y_1)$ is tangent to the homoclinic orbit at (u_1, y_1). But the flow Φ^O maps tangent vectors to tangent vectors, so $\Phi^O(\Phi^I(\beta^O)(u_1, y_1))(u_{\max}, 0)$ is vertical in this case, so in this case one can see directly that $A_3 \geqslant 1$.

Lastly if $\Phi^I(\beta^O)(u_1, y_1) \times b^O(u_1, y_1) < 0$, then denote $b^O(u_{\max}, 0) := (0, -a)$ where a is some positive number. We then have

$$0 > \Phi^O(\Phi^I(\beta^O)(u_1, y_1))(u_{\max}, 0) \times (0, -a) = (-a)\Phi_1^O(\Phi^I(\beta^O)(u_1, y_1))(u_{\max}, 0).$$

This means that the first coordinate of the image of the vector under the flow is positive, so the vector must have passed through the vertical at some point. Thus $A_1 + A_2 + A_3 \geqslant 2$ in this case as well.

So we have that for solutions of this type the number of zeros of the associated variational equation is greater than or equal to two. This completes the proof of the theorem. □

Remark 1. Solutions shown in figures 3(*b*) and (*c*) (see also the corresponding phase portraits in figures A1(*b*) and (*c*)) belong, respectively, to case 1 and 2 in the proof of theorem 2. Let $\varsigma \in \mathbb{R}$ be the real part of a λ in the spectrum of D_+ such that $D_+v(x) = \lambda v(x)$. In figure 10 we plot the numerically obtained spectral parameter $\varsigma > 0$ of symmetric solutions along the upper branch of figure 2 as a function of ω, from which one can see that $P = 2$ indeed.

So far we have been primarily concerned with positive solutions to (3), but theorem 1 applies equally well to standing waves $u(x)$ which are not strictly positive, so long as they are smooth enough and both u and u_x tend to 0 as $x \to \pm\infty$. Likewise, the techniques used to calculate P in the proof of theorem 2 do not require that the solution be positive. As such, we can apply theorem 1, and the techniques above to establish the linear instability of some excited states with $Q \geqslant 1$. The first excited standing wave we will deal with has $Q = 1$.

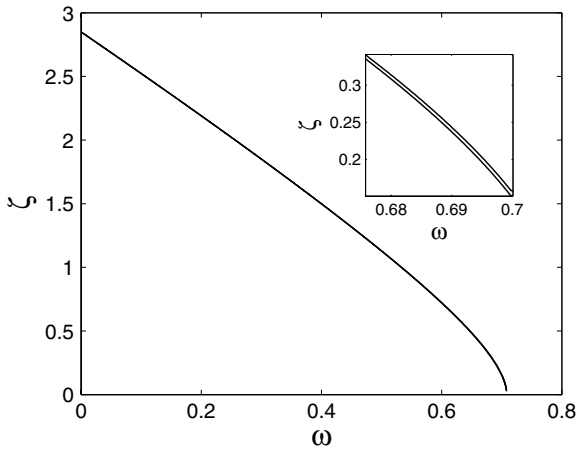

Figure 10. The spectrum $\varsigma > 0$ of D_+ for unstable symmetric solutions along the upper branch in figure 2 as a function of ω. The inset zooms in on a small region clearly showing that there are two curves.

4.2. First excited unstable states

We will consider steady-state solutions with the following properties

(i) The switch from the outer to the inner system takes place in the phase plane at (u_0, y_0), with $y_0 < 0$ and $0 < u_0 < \sqrt{V/2}$.
(ii) The solution returns to the outer homoclinic orbit at the point $(u_1, y_1) = (-u_0, y_0)$.

Such a solution will be symmetric with respect to the y-axis in the phase plane, and such solutions exist for all values of V and ω. An example of the phase portrait of such a solution can bee seen in figure 11(a).

Corollary 4. *Let $u(x)$ be as above, then $P \geqslant 3$ and so we have a linearly unstable standing wave to equation (1).*

In order to prove the corollary, we need the following lemma, which is the analogue to lemma 3 in the half of the phase plane where $u < 0$.

Lemma 5. *If $d(u, y)$ is a vector in the tangent space to the phase plane of the homoclinic orbit at the point (u, y), with $u < 0$ such that $d(u, y) \times b^O(u, y) > 0$, then*

$$\lim_{x\to\infty} \Phi^O\left(\frac{d}{|d|}\right)(F^O(u, y)) = k\begin{pmatrix} 1 \\ \sqrt{V-\omega} \end{pmatrix}, \tag{25}$$

where k is a negative real number.

The proof is exactly the same as in the proof of lemma 3, except that

$$\lim_{x\to\infty} \Phi^O\left(\frac{b^O}{|b^O|}\right)(F^O(u, y)) = \lim_{x\to\infty} \frac{b^O}{|b^O|}(F^O(u, y)) = \frac{1}{-\sqrt{1+V-\omega}}\begin{pmatrix} -1 \\ \sqrt{V-\omega} \end{pmatrix} \tag{26}$$

because we are in the left half plane. This change of sign therefore changes the sign of k.

It is straightforward to calculate that $A_1 \geqslant 1$. This is done in exactly the same way as in the proof of the second case of theorem 2. Similarly, as in the second case of theorem 2, one shows that $A_1 + A_2 + A_3 = P \geqslant 3$. This is done by using the cross product of the appropriate

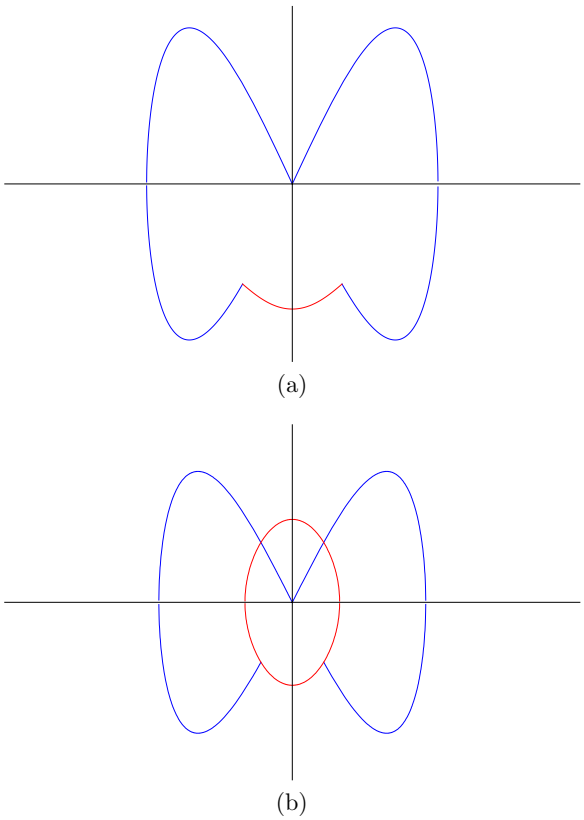

Figure 11. (*a*) An unstable orbit where $P = 3$ and $Q = 1$. (*b*) An unstable orbit where $P = 2k+3$ and $Q = 2k+1$ and $k \geqslant 1$. The number k describes the number of periods the solution stays in the inner periodic orbit.

vectors under the flows of the outer system, showing that the first coordinate of the tangent vector under the flow of the variational equation is first positive, then negative, then positive and finally ends up negative because of lemma 5. These three sign changes mean that the vector has passed through the vertical at least three times, and hence we have an unstable standing wave.

Remark 2. The solution shown in figure 6(*a*) (see the corresponding phase-portrait in figure A2(*a*)) belongs to the class of solutions discussed in corollary 4. Nevertheless, the symmetric solution corresponding to point C in figure 5 (cf figure 6(*c*) and its phase-portrait A2(*c*)) does not belong to the same class of solutions. In the phase-space, the orbit of the latter solution is sketched in figure 12(*a*). This is similar to the configuration of the orbit in corollary 4, which is a symmetric (about the u-axis) solution in the phase space with the properties $\omega/V < 2/3$, $y_0 < 0$ and $(u_1, y_1) = (-u_0, y_0)$, but here $u_0 < \sqrt{V/2}$. In this case, the inner orbit lies outside the heteroclinic orbit of the inner system. In this configuration, we have that $Q = 1$ and $P \geqslant 2$. This implies that the above method cannot be used to prove the instability of such a solution. In figure 12(*b*), we plot the numerically obtained positive spectrum $\varsigma > 0$ of the operator D_+ for unstable symmetric solutions in figure 5, where one can see that $P = 3$ only in some interval. We conjecture that the break down of our method occurs at the points where the branch containing point B and that containing points D and E emerge with the main branch corresponding to symmetric solutions.

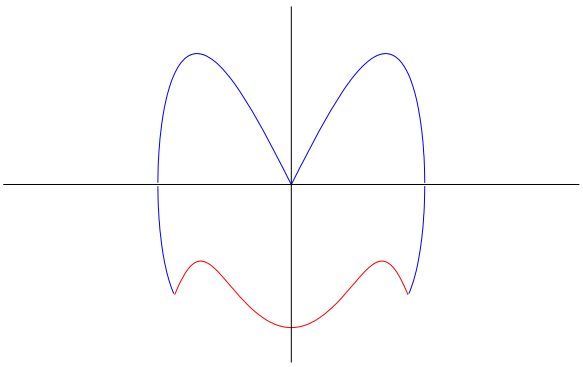

(a)

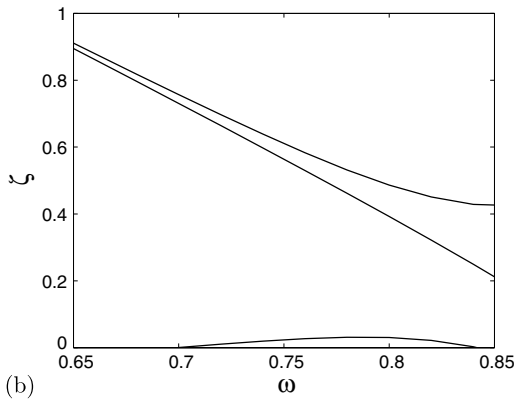

(b)

Figure 12. (*a*) A sketch of symmetric orbits with $P \geqslant 2$ and $Q = 1$. (*b*) The same as in figure 10, but for unstable symmetric solutions in figure 5.

4.3. Higher order excited states

We remark that there are certain choices of V and ω, and u_0 such that the inner part of the superimposed phase portrait will be part of a periodic orbit of the inner system. This applies, for example, if we keep the (u_0, y_0) and $(u_1, y_1) = (-u_0, y_0)$ as in corollary 4. We can allow the trajectory to follow the periodic orbit for as many periods as we like, and can calculate the net effect on the stability of the standing wave as a whole. One can show that if the base point travels along the inner orbit described by (16) from (u_1, y_1) for exactly one period, the solution to the variational equation will have exactly two more zeros, as will the original solution. Thus for each period $P = Q = 2$, and so we still have an unstable excited solution. In this way we are capable of constructing unstable excited solutions with $2k + 1$ zeros for an arbitrary k. Figure 11(*b*) is a phase portrait for such a standing wave solution.

It remains to determine which choices of V, w and u_0 will produce such an excited state. Using the geometry of the superposed phase portraits we have that such an excited steady-state solution will exist when

$$\begin{aligned} &\frac{\omega}{V} < \sqrt{\frac{1}{2}} \qquad \text{and} \qquad u_0 < \sqrt{\frac{V - \sqrt{V^2 - 2\omega^2}}{2}} \quad \text{or} \\ &\frac{\omega}{V} > \sqrt{\frac{1}{2}} \qquad \text{and} \qquad u_0 < \sqrt{\frac{V}{2}}. \end{aligned} \tag{27}$$

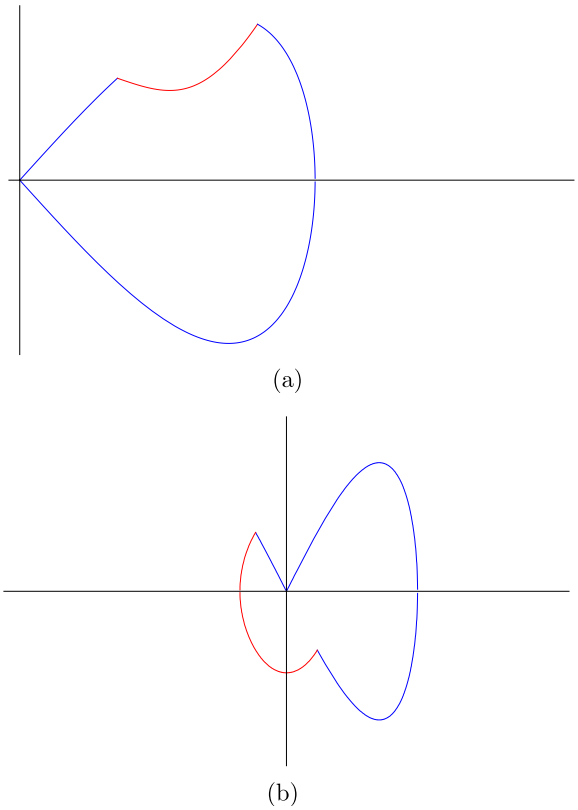

Figure 13. (*a*) An asymmetric orbit with $P \geqslant 1$ and $Q = 0$. (*b*) An asymmetric orbit with $P = 2$ and $Q = 1$.

The above technique can be used to create a higher order excited state whenever the inner part of the phase curve is part of a periodic orbit. We can simply follow the period as many times as is necessary and the higher order state will have the same difference of P and Q. Thus if we begin with an unstable state where $P = P_0$ and $Q = Q_0$ being the initial values for P and Q and the inner part of the orbit is periodic (for another example cf figure 9(*a*)), we can produce higher order unstable states with $P = 2k + P_0$ and $Q = 2k + Q_0$, and for all integer values of k we will still have an unstable state.

5. Asymmetric states

The techniques described and used in the section above cannot be applied to the asymmetric states considered in this paper because such states do not satisfy the condition in theorem 1. As particular examples, we consider two solutions with $Q = 0$ and $Q = 1$.

For positive solutions $Q = 0$, when $\omega/V < 3/4$, asymmetric orbits will be present. An example of the phase portrait of a positive asymmetric solution is in figure 13(*a*). For this case, it can be calculated that $P \geqslant 1$. The profile shown in figure 3(*c*) with its phase portrait depicted in figure A1(*c*) belongs to this class of asymmetric solutions. As we know numerically that asymmetric positive solutions are stable (see figure 3), it is expected that theorem 1

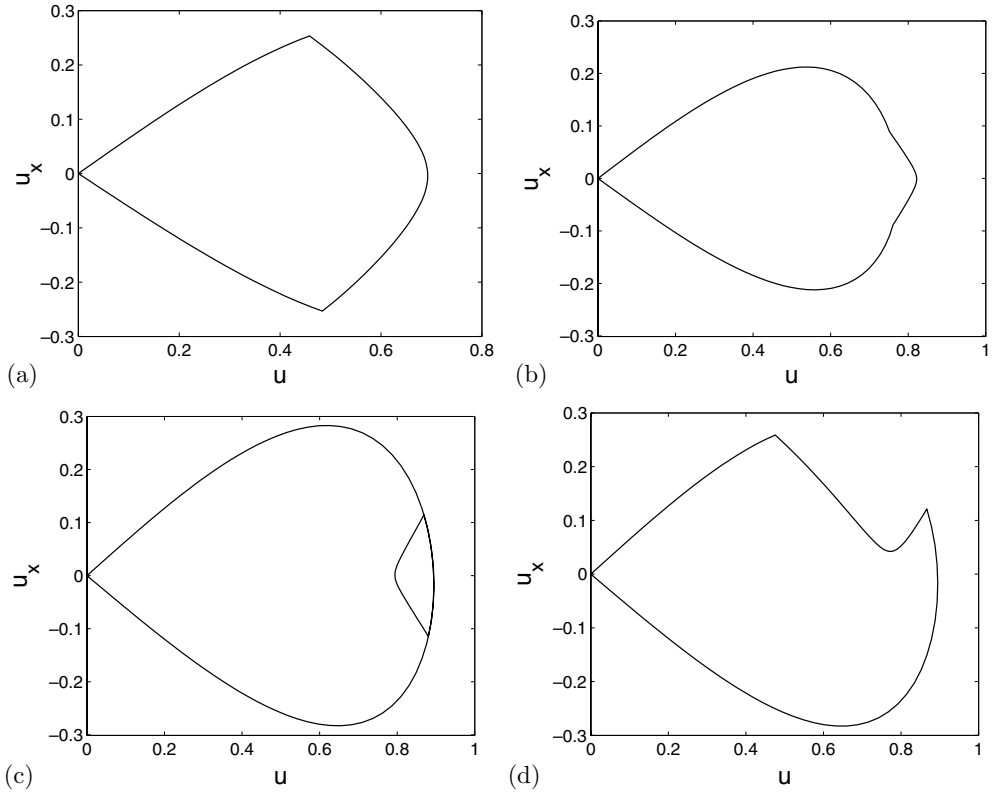

Figure A1. Phase portraits of solutions at points indicated as A–D in figure 2 (see also figure 3).

should not apply here. It is then interesting to know whether the stability can be established analytically.

Numerically (not shown here) we observed that $P = 1$ for the asymmetric positive state. If one could show analytically that $P = 1$ indeed, one would be able to prove the stability using the theorem presented in [41]. Nonetheless, the solution stability is expected and predicted using the method of [25].

Excited asymmetric orbits where $P = 2$ and $Q = 1$ can occur for all configurations of V and w. Such an orbit is described by the following properties. If $\omega/V < 3/2$, then for the point of departure (u_0, y_0), we have that $u_0 < \sqrt{V/2}$ and $y_0 < 0$. The orbit then travels through the y-axis in the phase plane and reconnects with the outer orbit at the point (u_1, y_1) where $u_1 < 0$ and $y_1 > 0$. Moreover, in this configuration of V and ω, the only type of inner orbit that can produce such an asymmetric solution happens to be periodic and symmetric about the line $y = u$ in the phase plane. Thus $(u_1, y_1) = (-u_0, -y_0)$, and the original vector tangent to the homoclinic orbit (β^O) gets mapped by the variational flow of the inner orbit to the tangent space of the homoclinic orbit at the point (u_1, y_1). Thus we know

$$\lim_{x\to\infty} \frac{\Phi^O(\Phi^I(\beta^O)(u_1, y_1))(u, y)}{|\Phi^O(\Phi^I(\beta^O)(u_1, y_1))(u, y)|} = \begin{pmatrix} -k \\ k\sqrt{V-\omega} \end{pmatrix}.$$

That is the limit under the variational flow of the vector which was originally tangent to the homoclinic orbit is the stable subspace of the variational flow at the critical point at the origin.

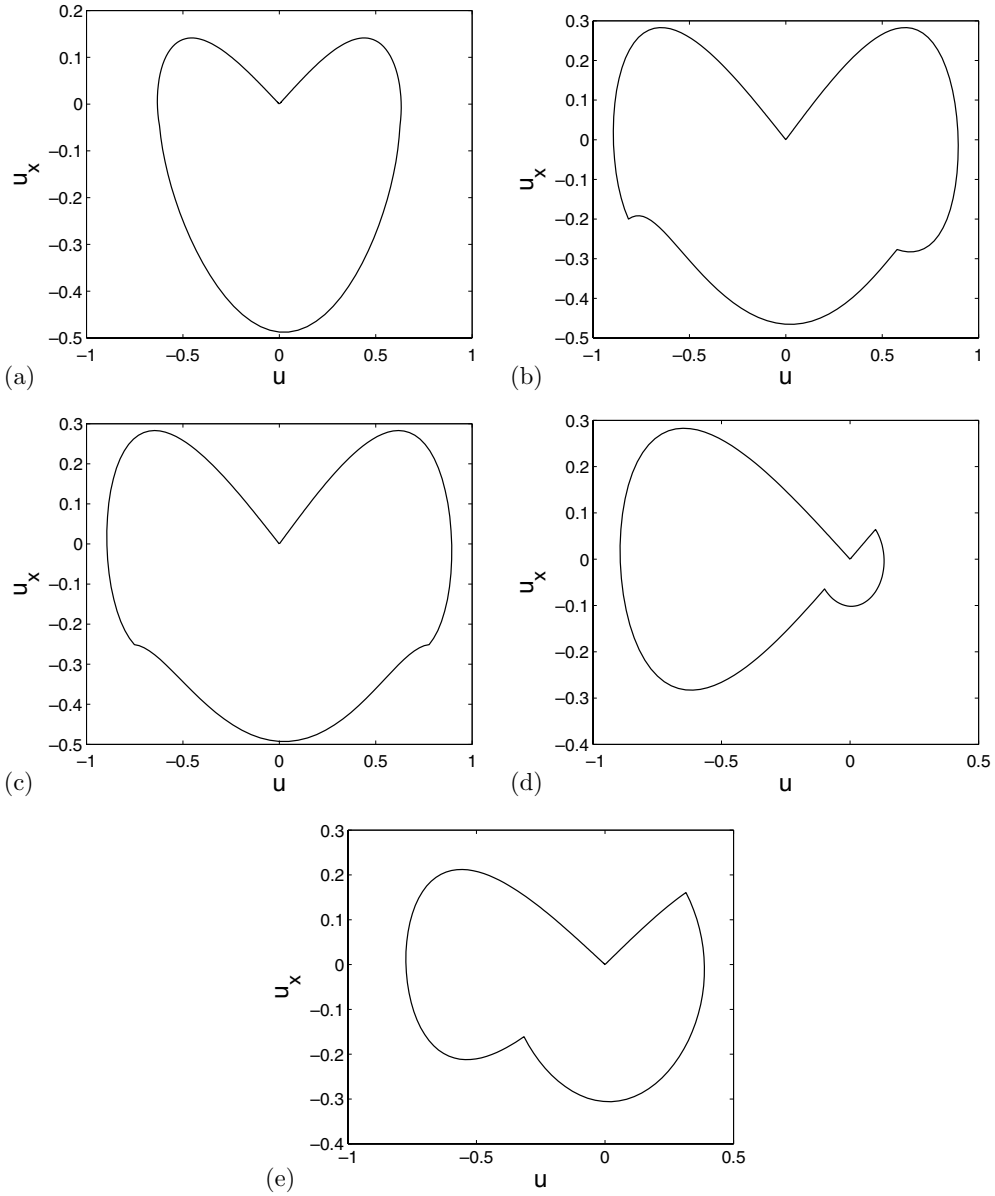

Figure A2. The same as figure A1 for solutions at points indicated as A–D in figure 5 (see also figure 6).

We can therefore only conclude that P is exactly 2. If we are in the case where $\omega/V > 3/2$ and $0 < u_0 < \sqrt{V/2}$, then we can exploit the same symmetry conditions as above for such asymmetric solutions, even concluding the limit of the variational solution under the tangent flow as the stable subspace of the critical point at the origin. An example of one such orbit is in figure 13(b), which is a sketch of the profile shown in figures 6(d) and (e). If, however, $\omega/V > 3/2$ and $u_0 > \sqrt{V/2}$, then no such periodic orbits exist, i.e. there is no connected inner orbit where (u_0, y_0) and (u_1, y_1) could have the aforementioned properties.

6. Summary

We have considered a nonlinear Schrödinger equation with a non-uniform nonlinearity coefficient. In particular, we have investigated a Schrödinger equation with self-defocusing nonlinearity bounded by self-focusing one. This work extended the results of [22, 25, 41]. We have established analytically the instability of symmetric states beyond a critical norm through the application of a topological argument developed in [16]. Even though the technique does not definitively establish instability in the case of the asymmetric states considered in this paper, we have numerically established the stability of some positive asymmetric states.

It is natural to extend the study to the case when the inhomogeneities are periodic. Recently, the same phase space method has been used to analytically construct gap solitons of the nonlinear Kronig–Penney model in a photonic structure [18–20]. The stability of such gap solitons is proposed to be studied in the future using analytical methods presented herein.

Acknowledgments

RM and CKRTJ were partly supported by ONR grant N000140910235 and NSF grant DMS-041026.

Appendix A. Phase portraits

In figure 3, the solution profiles corresponding to points A–D in figure 2 are shown in the physical space. The corresponding phase portraits of the solutions are presented in figure A1. The phase portraits of solutions shown in figure 6 are depicted in figure A2.

References

[1] Agranovich V M, Babichenko V S and Chernyak V Ya 1980 Nonlinear surface polaritons *Pis. Zh. Eksp. Teor. Fiz.* **32** 532
Agranovich V M, Babichenko V S and Chernyak V Ya 1980 *JETP Lett.* **32** 512
[2] Akhmediev N N 1982 Novel class of nonlinear surface waves: asymmetric modes in a symmetric layered structure *Pis. Zh. Eksp. Teor. Fiz.* **83** 545
Akhmediev N N 1982 *Sov. Phys.—JETP* **56** 299
[3] Anderson M H, Ensher J R, Matthews M R, Wieman C E and Cornell E A 1995 Observation of Bose–Einstein condensation in a dilute atomic vapor *Science* **269** 198201
[4] Boardman A D, Egan P, Lederer F, Langbein U and Mihalache D 1991 *Nonlinear Surface Electromagnetic Phenomena* ed V M Agranovich *et al* (New York: Elsevier Science Publishers B.V.) pp 73–287
[5] Bradley C C, Sackett C A and Hulet R G 1997 *Phys. Rev. Lett.* **78** 985
[6] Bose S N 1924 Plancks gesetz und lichtquantenhypothese *Z. Phys.* **26** 178
[7] Cazenave T 2003 *Semilinear Schrödinger Equations* (*Courant Lecture Notes in Mathematics* vol 10) (New York: N.Y.U Courant Institute)
[8] Davis K B, Mewes M-O, Andrews M R, van Druten N J, Durfee D S, Kurn D M and Ketterle W 1995 Bose–Einstein condensation in a gas of sodium atoms *Phys. Rev. Lett.* **75** 3969–73
[9] Einstein A 1924 Quantentheorie des einatomigen idealen gases. Part I *Sber. Preuss. Akad. Wiss.* **22** 261–7
Einstein A 1925 Quantentheorie des einatomigen idealen gases. Part II *Sber. Preuss. Akad. Wiss.* **1** 314
[10] Grillakis M, Shatah J and Strauss W 1987 Stability theory of solitary waves in the presence of symmetry. I *J. Funct. Anal.* **74** 160–97
[11] Gross E P 1961 Structure of a quantized vortex in boson systems *Nuovo Cimento* **20** 454–7
[12] Guckenheimer J and Holmes P 1983 *Nonlinear Oscillations, Dynamical Systems, and Bifurcations of Vector Fields* (*Applied Mathematical Sciences* vol 42) ed F John *et al* (New York: Springer)
[13] Jackson R K and Weinstein M I 2004 Geometric analysis of bifurcation and symmetry breaking in a Gross–Pitaevskii equation *J. Stat. Phys.* **116** 881–905
[14] Jensen S M 1982 The nonlinear coherent coupler *IEEE J. Quantum Electron.* **QE-18** 1580
[15] Jones C K R T and Moloney J V 1986 Instability of standing waves in nonlinear optical waveguides *Phys. Lett.* A **4** 117

[16] Jones C K R T 1988 Instability of standing waves for non-linear schrödinger-type equations *Ergod. Theory Dyn. Syst.* **8** 119–38
[17] Kolokolov A A 1973 *Lett. Nuovo Cimento Soc. Ital. Fis.* **8** 197
[18] Kominis Y and Hizanidis K 2006 Lattice solitons in self-defocusing optical media: analytical solutions of the nonlinear Kronig–Penney model *Opt. Lett.* **31** 2888–90
[19] Kominis Y 2006 Analytical solitary wave solutions of the nonlinear Kronig–Penney model in photonic structures *Phys. Rev.* E **73** 066619
[20] Kominis Y, Papadopoulos A and Hizanidis K 2007 Surface solitons in waveguide arrays: analytical solutions *Opt. Express* **15** 10041–51
[21] Lederer F, Stegeman G I, Christodoulides D N, Assanto G, Segev M and Silberberg Y 2008 Discrete solitons in optics *Phys. Rep.* **463** 1–126
[22] Leon J 2004 Nonlinear tunneling in a fiber guide array resonator *Phys. Rev.* E **70** 056604
[23] Lomtev A I 1981 A new class of nonlinear surface waves *Pis. Zh. Eksp. Teor. Fiz.* **34** 64
Lomtev A I 1981 *JETP Lett.* **34** 60
[24] Maradudin A A 1981 S-polarized nonlinear surface polaritons *Z. Phys.* B **41** 341–4
[25] Mitchell D J and Snyder A W 1993 Stability of fundamental nonlinear guided waves *J. Opt. Soc. Am.* B **10** 1572–80
[26] Morandotti R, Eisenberg H S, Silberberg Y, Sorel M and Aitchison J S 2001 Self-focusing and defocusing in waveguide arrays *Phys. Rev. Lett.* **86** 3296–9
[27] Perko L 2001 *Differential Equations and Dynamical Systems* (*Texts in Applied Mathematics* vol 7) ed J Marsden *et al* (New York: Springer)
[28] Pitaevskii L P 1961 Vortex lines in an imperfect Bose gas *Sov. Phys.—JETP* **13** 451–4
[29] Rodas-Verde M I, Michinel H and Pérez-García V M 2005 Controllable soliton emission from a Bose–Einstein condensate *Phys. Rev. Lett.* **95** 153903
[30] Sakaguchi H and Malomed B A 2005 Matter-wave solitons in nonlinear optical lattices *Phys. Rev.* E **72** 046610
[31] Seaton C T, Valera J D, Shoemaker R L, Stegeman G I, Chilwell J T and Smith S D 1985 Calculations of nonlinear TE waves guided by thin dielectric films bounded by nonlinear media *IEEE J. Quantum Electron.* **QE-21** 774
[32] Shatah J and Strauss W 1985 Instability of nonlinear bound states *Commun. Math. Phys.* **100** 173–90
[33] Sivan Y, Fibich G, Ilan B and Weinstein M I 2008 Qualitative and quantitative analysis of stability and instability dynamics of positive lattice solitons *Phys. Rev.* E **78** 046602
[34] Stegeman G I 1992 *Contemporary Nonlinear Optics* ed B P Agrawal and R W Boyd (New York: Academic) pp 1–37
[35] Sukhorukov A A, Kivshar Yu S, Bang O, Rasmussen J J and Christiansen P L 2001 Nonlinearity and disorder: classification and stability of nonlinear impurity modes *Phys. Rev.* E **63** 036601
[36] Sulem C and Sulem P-L 1999 *Nonlinear Schrödinger Equations: Self-Focusing and Wave Collapse* (*Applied Mathematical Sciences* vol 139) ed J E Marsden and L Sirovich (New York: Springer)
[37] Theocharis G, Schmelcher P, Kevrekidis P G and Frantzeskakis D J 2005 Matter-wave solitons of collisionally inhomogeneous condensates *Phys. Rev.* A **72** 033614
[38] Theocharis G, Schmelcher P, Kevrekidis P G and Frantzeskakis D J 2006 Dynamical trapping and transmission of matter-wave solitons in a collisionally inhomogeneous environment *Phys. Rev.* A **74** 053614
[39] Tomlinson W J 1980 Surface wave at a nonlinear interface *Opt. Lett.* **5** 323–5
[40] Tran H T 1992 Stability of bright TE waves in slab waveguides with a self-defocusing bounding medium *Opt. Lett.* **17** 1767–9
[41] Tran H T 1992 Stability of TE_0 modes in self-defocusing core nonlinear planar waveguides *Optics Commun.* **93** 202–6
[42] Tran H T and Ankiewicz A 1992 Instability regions of nonlinear planar guided waves *IEEE J. Quantum Electron.* **28** 488
[43] Tran H T, Mitchell J D, Akhmediev N N and Ankiewicz A 1992 Complex eigenvalues in stability analysis of nonlinear planar guided waves *Optics Commun.* **93** 227–33
[44] Vakhitov M G and Kolokolov A A 1973 Stationary solutions of the wave equation in the medium with nonlinearity saturation *Izv. Vyssh. Uchebn. Zaved. Radiofiz.* **16** 1020
Vakhitov M G and Kolokolov A A 1973 *Radiophys. Quantum Electron.* **16** 783
[45] Weinstein M 1985 Modulational stability of ground states of nonlinear Schrödinger equations *SIAM J. Appl. Math.* **16** 472–91
[46] Zezyulin D A, Alfimov G L, Konotop V V and Pérez-García V M 2007 Control of nonlinear modes by scattering-length management in Bose–Einstein condensates *Phys. Rev.* A **76** 013621